

Comparison of 60 GHz and 80 GHz Vehicle-to-Vehicle Channels Using Delay and Doppler Characteristics

Ales Prokes*, Tomas Mikulasek*, Josef Vychodil*, Radek Zavorcka*, Jiri Blumenstein*, Jaroslaw Wojtun[‡], Jan M. Kelner[‡], Cezary Ziolkowski[‡], Aniruddha Chandra[†]
[‡]Institute of Communications Systems, Military University of Technology, Warsaw, Poland;
[†]ECE Department, National Institute of Technology, Durgapur, India;
^{*}Brno University of Technology, Brno, Czechia, Email: prokes@vut.cz

Abstract—The aim of this paper is to provide a comparison of channel characteristics for vehicle-to-vehicle (V2V) communication at 60 GHz and 80 GHz frequency bands in a high-mobility scenario where two vehicles pass each other in opposite directions. The study is based on measurements of the time-varying channel impulse response capturing the behavior of multi-path propagation during vehicle motion. By directly comparing these two frequency bands under identical measurement conditions, we attempt to quantify the differences in power delay profile, root mean square (RMS) delay spread, RMS Doppler spread, and intervals (regions) of stationarity in time domain. The results show that these bands do not differ significantly, but the 80 GHz band exhibits somewhat greater RMS delay spread and RMS Doppler spread when calculated over the entire delay-Doppler spectrum, and conversely exhibits shorter stationarity regions. However, the characteristics of the measurement setup in the two bands and their influence on comparative measurements must be considered. In particular, attention must be paid to the impact of antennas.

Index Terms—V2V channel, millimeter wave, channel impulse response, delay-Doppler spectrum, delay spread, stationarity regions

I. INTRODUCTION

The demand for higher data rates, lower latency, and greater reliability in wireless communications has driven the exploration of new frequency bands and novel communication paradigms. Millimeter wave (mmWave) bands, typically defined between 30 GHz and 300 GHz, offer large unused bandwidths and have been identified as a key enabler for next-generation wireless systems, including 5G and beyond. However, signal propagation in mmWave bands poses significant challenges due to higher free-space path loss, sensitivity to blockages, limited diffraction, and fast temporal variations in dynamic environments. Accurate modeling of the radio channel is therefore essential to understand and mitigate these effects, especially in applications where reliability and performance are tightly coupled to the physical environment.

A particularly challenging application is high-mobility vehicle-to-vehicle (V2V) communication, where both the transmitter and receiver located on vehicles are moving at high relative speeds, causing rapid channel changes, Doppler effects, and time-varying multi-path propagation. These effects

are especially pronounced at mmWave frequencies, where channel behavior strongly depends on vehicle geometry, trajectory, antenna orientation, and surrounding objects.

Several recent works have focused on characterizing V2V channels in the mmWave bands based on real measurements. For example, [1] provides a detailed overview of the V2X channel analyzes in various scenarios (passing vehicles, overtaking, convoy driving, and driving in urban environments), describing sounder setups and comparing key channel parameters such as delay, Doppler, and angular spread, path loss, stationarity regions, and others. It highlights how channel characteristics relate to different driving situations. In [2], V2V channel measurements at 73 GHz were performed in an urban environment with vehicles approaching at 60 km/h. The study analyzes large-scale and small-scale fading, showing that the fast-fading distribution evolves from Rician to Nakagami and eventually to lognormal as the Tx–Rx distance increases. Similarly, the authors in [3] provides real traffic measurements using a double-directional 60 GHz sounder ReRoMA in scenarios such as convoys, oncoming traffic and overtaking and presents key channel parameters such as the path loss exponent (1.9), the RMS delay spread (5–110 ns), and angular spread (0.05–0.4 rad). Extensive 41 GHz V2V measurements in urban and underground parking scenarios examined vehicle obstructions are presented in [4]. A stochastic path loss model is proposed for both line-of-sight (LOS) and obstructed LOS. The influence of certain obstacles is being investigated. For example, an obstacle in the form of truck adds 9–19 dB path loss and reduces shadow fading deviation by 1–2 dB, depending on distance to the RX. A new V2V path loss model based on 59.6 GHz measurements in crossing-vehicle scenarios, offering improved accuracy over traditional models for both approaching and receding vehicles is published in [5]. Paper [6] presents a 1 GHz-wide V2V channel sounder operating at 28 GHz, using phased arrays to capture 116 directional beams in less than 1 ms. When measured on highways and in urban environments, it revealed rich scattering, directional diversity, and waveguide-like effects that increase the reliability and range of mmWave V2V. Ref. [7]

presents initial V2V measurement results at 26 GHz in urban and suburban areas with different movement scenarios. The analysis includes time-varying power delay profiles, path loss, and delay spread, which ranges from 25 to 150 ns depending on the environment. Another study [8] measures 60 GHz path loss between vehicles on urban highways and roads, showing distance-dependent attenuation that follows a 2nd-order power law on highways and 1st-order on city streets. It reports extra losses of 15 dB on highways and 5 dB on local roads beyond 30 m and confirms V2V communication feasibility out to beyond 100 m. Multiband V2V measurements across several frequency bands (6.75 GHz, 30 GHz, and 60 GHz) in a street canyon environment is presented in [9]. It analyses path loss, delay spread, and angular spread in different traffic conditions. It highlights how channel metrics vary with frequency, revealing richer scattering and reduced coherence at higher bands. In [10] the authors provide V2V propagation data measured at a T-intersection across the same frequencies as above, showing strong frequency-dependent behavior in path loss and multi-path richness due to building and vehicle blockage. In paper [11], a 60 GHz vehicle-to-infrastructure (V2I) radio channel in a suburban environment is characterized by channel transfer function (CTF). The transmitter was mounted on a moving vehicle. Doppler spread function demonstrated the effects of nearby parked vehicles. Propagation loss between two moving vehicle at 60 GHz was studied in [12] with up to three commercial vehicles blocking the LOS. Models were developed to represent NLOS propagation characteristics. V2V measurements across 6.75, 30, 60, and 73 GHz in urban and highway settings focusing on vehicle blockage showed that blocking vehicle causes 5.5–17 dB loss, and increased delay and angular spreads depending on blocker size [13]. Note that there are other similar works carried out by teams such as NYU Wireless.

Although these studies provide valuable insights, they often focus on static or less mobile configurations, or concentrate on a single frequency band, which limits the generality of their conclusions. A closer study of the above-mentioned and other works would reveal that the channel sounders used for measurements often have a limited bandwidth not exceeding 1 GHz, which limits the time resolution of the measurements, and have a small memory depth for recordings lasting barely a few seconds. Channel analyses are dominated by path loss characteristics influenced by distance or the environment (blocking objects). Small-scale channel features such as RMS delay spread, angle spread, and statistical properties such as power delay profile (PDP) or channel impulse response (CIR) fitting with different distributions are sometimes presented, but characteristics such as RMS Doppler spread or stationarity regions are rarely mentioned, even though they are very important for understanding channel variability over time, which is critical for system design, channel estimation, and beamforming efficiency.

This paper aims to contribute to this area by providing

- *Comparative analysis at 60 GHz and 80 GHz mmWave*

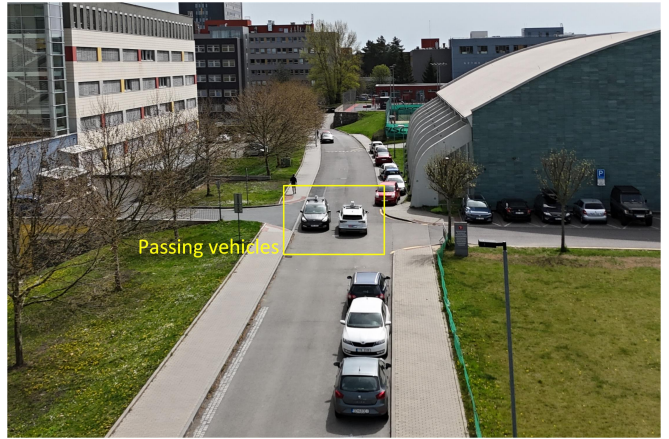


Fig. 1: Measurement V2V scenario for passing vehicles in the opposite direction at BUT



Fig. 2: Measuring vehicle with channel sounder transmitters mounted on the roof of the vehicle

bands: The study examines V2V channel behavior under identical measurement conditions in a high-mobility scenario with vehicles passing in opposite directions.

- *Long-time CIR analysis with excellent delay-domain resolution*: Channel measurements with 2 GHz bandwidth provide detailed analysis of multi-path propagation, and large memory depth enables examination of channel characteristics evolution in delay and Doppler domains.
- *Quantitative comparison of key parameters*: The paper compares RMS delay spread, RMS Doppler spread, and stationarity regions, under identical conditions to highlight frequency-specific differences.

The rest of the paper is structured as follows: Section 2 provides an overview of the measurement scenarios. Section 3 briefly describes the measurement setup. Section 4 outlines the methods used for signal processing. Section 5 presents the results of the measurements, simulations and the calculation of channel parameters. Finally, the conclusion summarizes the key findings of the paper.

II. MEASUREMENT SCENARIO

The measurement of passing vehicles was carried out on the campus of the Faculty of Electrical Engineering and Commu-

nication Technologies of the Brno University of Technology between the building at Technická 12, the sports complex, and the parking lot (see Fig. 1 and <https://mapy.com/s/goculagone>). Near the road within the measurement range, there are parked cars, streetlights, traffic signs, medium-sized trees, and sports complex building. The pillars and wall of the building are approximately 3 m and 6.5 m away from the road. The wall of the building is 9 m high. The road is approximately 6 m wide and the sidewalks on both sides are 2 m wide. Omnidirectional antennas and outdoor units for channel measurement were mounted on the roofs of the vehicles. The location of the transmitting units on the Škoda Eniaq car is shown in Fig. 2 (the 80 GHz unit is located at the front). The receiving units of the sounder are mounted similarly to the Ford Galaxy car.

In this paper, we present the results of two measurements of passing cars. During the first measurement, the cars passed each other at the location shown in the Fig. 1. During the second measurement, the passing location was approximately 20 meters further away, i.e., closer to the sports complex. In the first measurement, the speed of the cars was approximately 30 km/h and 50 km/h, and in the second measurement it was approximately 35 km/h and 45 km/h. The first measurement is described in detail, including graphs and an overview of selected parameters. Due to limited space, the second measurement is presented only as the overview of channel parameters.

III. MEASUREMENT SETUP

The 60 GHz and 80 GHz bands were used due to the availability of components (antennas, amplifiers, and converters) and because they are the subject of research in projects 23-04304 and MubaMilWave (see Acknowledgement).

The channel sounder employs a Xilinx Zynq UltraScale+ RFSoc ZCU111 board as the base-band transmit subsystem for the both bands. It generates a frequency modulated continuous wave (FMCW) signal with ramp-up and ramp-down in order to make the spectrum as flat as possible. The 8 s duration of FMCW segment enables up to 125.000 measurements per seconds and the bandwidth 2.048 GHz offers distance resolution of 15 cm. Using SiversIMA FC1003E converters, this signal is up- and down-converted between baseband and the 60 GHz and 80 GHz bands. The transmitted signals are amplified by Filtronic Cerus 4 power amplifiers (PAs) at 80 GHz band and Quinstar (product line QPW) at 60 GHz band. The 60 GHz and 80 GHz received signals are amplified by low noise amplifiers (LNAs) Quinstar (product line QLW) and Low Noise Factory (product line LNF-LNR) respectively. The TD testbed has been optimized to significantly improve the sensitivity, IQ imbalances and dynamic range [14], which is about 45 dB. The transmitters (TXs) and receivers (RXs) are synchronized by Stanford Research Systems FS740 GPS/Rubidium reference clocks. For more information on the channel sounder architecture for 80 GHz and about the preprocessing of the FMCW signal response to obtain the CIR, see [15]. Note that the 60 GHz channel sounder

has the same architecture and uses similar components.

In order to justify any differences in the analysis results for both bands, it is necessary to consider the effects of key components in both frequency sections of the channel sounder. An overview of these components can be found in Table I.

IV. DATA PROCESSING METHODOLOGY

The basic function on which all further analyses are based and which is provided by the channel sounder is time-varying channel impulse response $h(t, \tau)$. It can be modeled as a sum of L multi-path components, where each path is characterized by a time-dependent amplitude $a_l(t)$, a phase shift $\phi_l(t)$, and a delay $\tau_l(t)$.

$$h(t, \tau) = \sum_{l=1}^L a_l(t) e^{j\phi_l(t)} \delta[\tau - \tau_l(t)]. \quad (1)$$

The function $\delta(\cdot)$ represents the Dirac delta. From the CIR we can simply get the *instantaneous* PDP

$$P(t, \tau) = |h(t, \tau)|^2 \quad (2)$$

that characterizes how received power is distributed across different propagation delays at given time t .

A. RMS delay and Doppler spreads

The RMS delay spread is a key parameter characterizing the temporal dispersion of a wireless channel. It is given as the standard deviations of the respective power distributions, computed directly from their first and second moments. It can be obtained from PDP for a given time t and i -th multi-path components (MPCs) [16]

$$\sigma_\tau(t) = \sqrt{\frac{\sum_i \tau_i^2 P(t, \tau_i)}{\sum_i P(t, \tau_i)} - \left[\frac{\sum_i \tau_i P(t, \tau_i)}{\sum_i P(t, \tau_i)} \right]^2}. \quad (3)$$

The resulting mean value shown in Table II is then obtained by averaging $\sigma_\tau(t)$ over all times.

To get the Doppler spread that characterizes the frequency dispersion of a wireless channel caused by relative motion between the transmitter and receiver, we need to first define delay-Doppler spectrum $S(\tau, \nu)$ also known as Doppler spreading function. It can be computed by applying the discrete Fourier transform along the time dimension for each fixed delay τ

$$S(\tau, \nu) = |\text{FFT}_t \{h(t, \tau)\}|^2. \quad (4)$$

Then the RMS Doppler spread is given similarly to (3) by the relation

$$\sigma_\nu(\tau) = \sqrt{\frac{\sum_k \nu_k^2 S(\tau, \nu_k)}{\sum_k S(\tau, \nu_k)} - \left[\frac{\sum_k \nu_k S(\tau, \nu_k)}{\sum_k S(\tau, \nu_k)} \right]^2}. \quad (5)$$

Two methods were used to estimate the RMS Doppler spread. In the first method (Method 1) the RMS Doppler spread is computed from the entire delay-Doppler spectrum $S(\tau, \nu)$

TABLE I: Comparison of channel sounder component parameters for the 60 GHz and 80 GHz bands

	60 GHz			80 GHz		
	PA	LNA	Antenna	PA	LNA	Antenna
Model	QPW-50662330-C1	QLW-50754530-I2	Cone-monopole (*)	Cerus 4 AA015	LNF-LNR55_96WA_SV	SAO-6039030230-12-S1
Frequency range [GHz]	50–66	50–75	50–67	81–86	55–96	60–90
Gain [dB, dBi]	30	31	0.6	21	27	2.0
Gain flatness/variation	±3	±3.5	±1.5	–	±2.5 (**)	±3.5
1dB [dBm] (***)	23	–	–	29	–	–
Transmitted power [dBm]	16	–	–	22	–	–
Noise figure [dB]	–	4.5	–	–	2.86	–
3 dB Vertical Beam-width	–	–	130°	–	–	30°

(*) Own design and manufacture. (**) For frequency above 56 GHz. (***) 1 dB compression point.

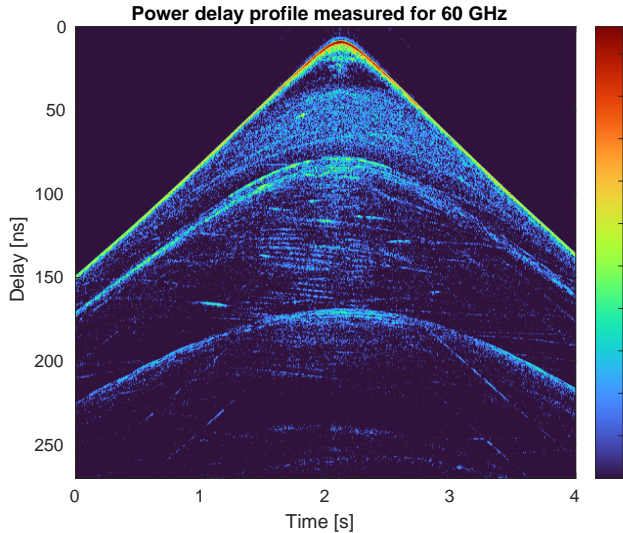


Fig. 3: Power delay profile of V2V channel measured in the 60 GHz band

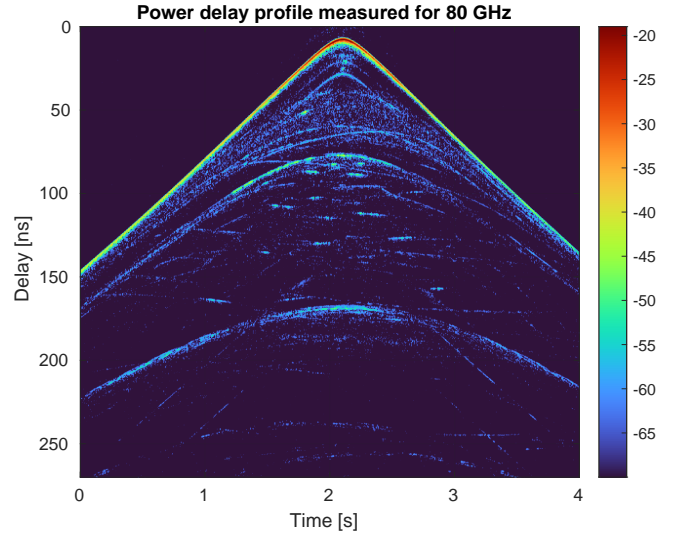


Fig. 4: Power delay profile of V2V channel measured in the 80 GHz band

according (5). The mean RMS Doppler spread shown in Table II is then obtained by averaging $\sigma_\nu(\tau)$ over all delays.

In the second method (Method 2) we calculate the delay Doppler spectra from $h(\tau, t)$ within a sliding time window with a certain width and a certain window shift step. In other words, a short-term Fourier transform (STFT) is applied to the time evolution of the channel impulse response $h(\tau, t)$. For each time window the RMS Doppler spread $\sigma_\nu(\tau)$ is calculated as with the Method 1. The final mean value is the average over all time windows. This second method shows us how the RMS Doppler spread develops during vehicle movement and is more illustrative. The disadvantage is that the window width limits the frequency resolution of the spread.

B. Stationarity regions

Stationarity regions can be identified by computing the Pearson correlation coefficient between adjacent PDPs or between PDPs at a fixed step size and tracked when the correlation drops below a predefined threshold (e.g., 0.9) [1]. This approach estimates the length of quasi-stationary intervals where channel statistics remain approximately constant. The step size must be chosen to account for the high temporal resolution of the measurements, ensuring sufficient channel variation between compared PDPs. A similar approach uses a sliding window in which CIR values are averaged and correlations are made between the averages. Another option for stationar-

ity evaluation is the local scattering function (LSF), which describes spectral power variations in the time–frequency domain. Stationarity can also be assessed through collinearity in time or frequency [17] or through the spectral distance of LSFs, using similarity thresholds. Also wide-sense-stationary (WSS) tests that compare second-order statistics [18] can be applied. For comparison purposes, we used the correlation of CIR taken at fixed intervals (every 50th CIR).

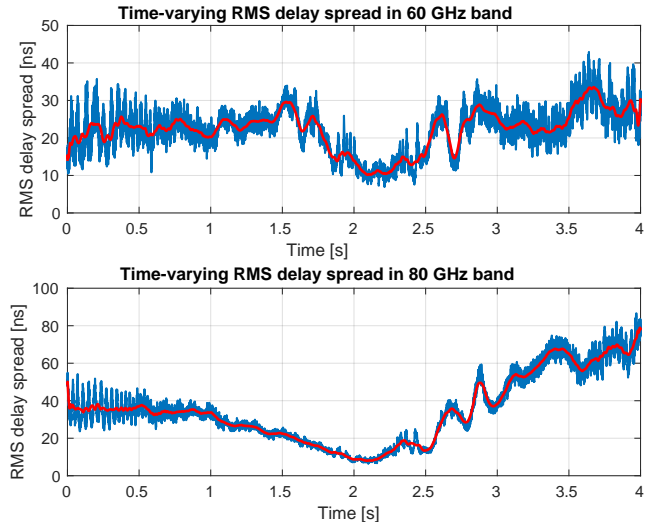


Fig. 5: Time-varying RMS delay spread in the 60 GHz band (top) and 80 GHz band (bottom)

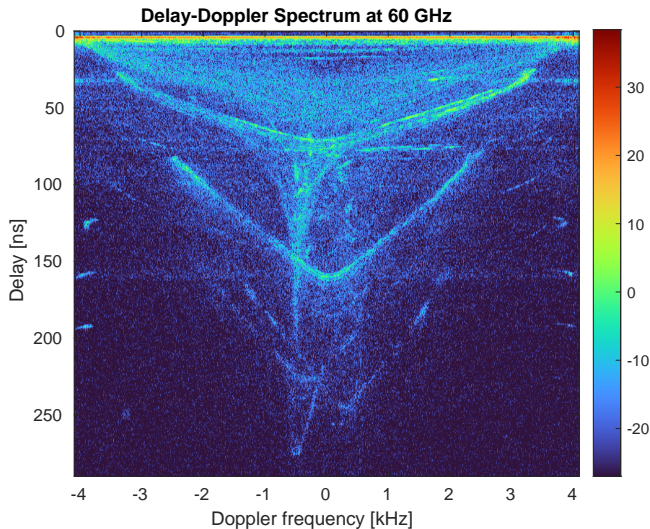


Fig. 6: Delay-Doppler spectrum for 60 GHz band

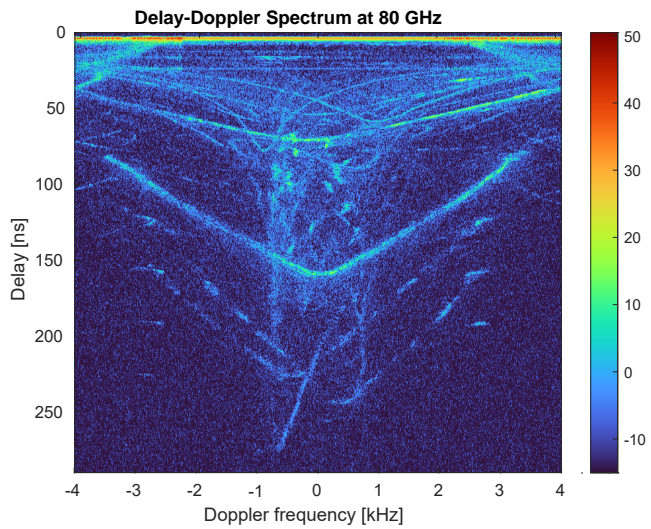


Fig. 7: Delay-Doppler spectrum for 80 GHz band

V. MEASUREMENT AND CALCULATION RESULTS

Before measurements, the channel sounder was calibrated by inserting an attenuator between the receiver and transmitter and recording the calibrated data for both frequency bands. The calibration data were then used for FMCW processing. The measured PDPs values in both bands do not differ significantly, as can be seen in Fig. 3 and Fig. 4. For the calculation, we used only a 4-second data segment from the total 8-second recording, where the multipath components have sufficient power. The delay range corresponds to a distance of approximately 0–80 m. The measured data was truncated below the noise threshold, which is about -70 dBm for both the bands. The figures show that the range between the noise peaks and the maximum value of the LOS component is approximately 45 dB, which corresponds to the dynamic range of the receiver. It is worth mentioning that the comparative measurements of the PDPs can be affected by different antenna vertical beam-width in 60 GHz band (see Tab. I) which can create different number of MPCs. Variations in gains (listed in the horizontal plane) must also be considered.

To ensure a consistent and physically meaningful computation of the RMS delay spread, the CIRs are time-aligned such that the LOS component appears at a fixed delay (typically $\tau = 0$, or close to 0) across all time instances. This compensates for the varying propagation distance due to vehicle motion and avoids artificial inflation of the delay spread caused by shifting LOS delays. This approach corresponds to a situation where the receiver is synchronized with the incoming LOS component. Calculated RMS delay spreads are shown in Fig. 5. Note that all one-dimensional plots in the text use blue color to display the described functional dependence and red color to show the trend obtained by a moving average filter.

The 80 GHz band exhibits greater dispersion. Although there appears to be a larger number of MPCs in the 60 GHz band, there is no greater dispersion of delays, probably due to their lower power. This can be observed, for example, below

the LOS maximum (below the peak of the curve). It is also clear that some MPCs are present at 60 GHz when the cars are closest to each other. This is probably due to reflection from the car body, which is irradiated over a larger area due to the large beam width in the vertical direction, which is 130° . The RMS delay spreads for both bands can also be compared using the mean and standard deviation (std) values listed in Table II.

In the next step, we calculated the delay-Doppler spectra according to (4) using the aligned CIR. These spectra, shown in Fig. 6 and Fig. 7, exhibit a similar structure, with higher Doppler spread evident at 80 GHz due to a more dispersed energy in the higher Doppler bins. In general, a higher carrier frequency should also cause higher Doppler shifts. This assumption is confirmed by the calculation of the RMS Doppler spread according to Method 1 (M1), as shown in Table II.

However, in order to get an idea of the changes in RMS Doppler spread during vehicle movement, we calculated the

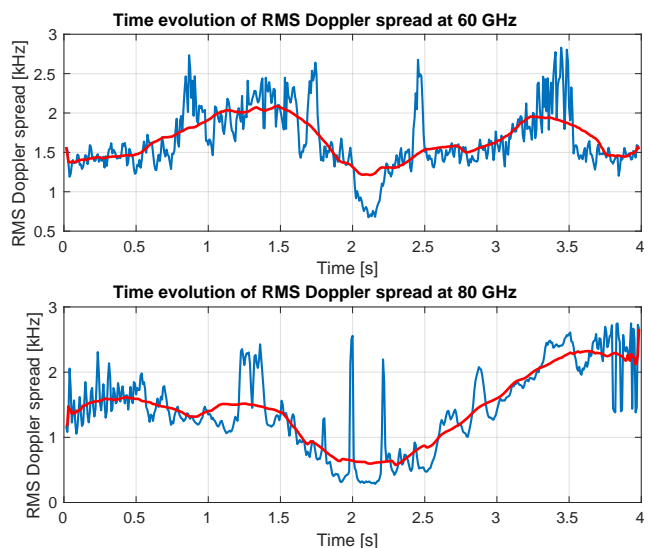


Fig. 8: Time-varying RMS Doppler spread for 60 GHz band (top) and 80 GHz band (bottom)

TABLE II: Selected channel parameters for two measurements

Measurement 1: Passing cars at the point shown in Fig. 1			
Parameter		60 GHz	80 GHz
RMS delay spread [ns]	mean	18.7	34.9
	std	5.94	18.2
RMS Doppler spread M1 [kHz]	mean	1.83	2.05
	std	0.44	0.45
RMS Doppler spread M2 [kHz]	mean	1.65	1.44
	std	0.39	0.63
Stationarity region [s]	mean	0.51	0.48
	std	0.30	0.23
Measurement 2: Passing cars at a point 20 m farther away			
Parameter		60 GHz	80 GHz
RMS delay spread [ns]	mean	22.1	38.9
	std	5.43	14.7
RMS Doppler spread M1 [kHz]	mean	1.91	2.16
	std	0.48	0.45
RMS Doppler spread M2 [kHz]	mean	1.81	1.57
	std	0.45	0.55
Stationarity region [s]	mean	0.47	0.42
	std	0.27	0.21

RMS Doppler spread according to Method 2. We chose a window length of 256 frequency bins and a step of 64 frequency bins. The result of the calculation is shown in Fig. 8. Here, the RMS Doppler spread for the lower frequency of the transmitted signal is higher, which does not correspond to the physical nature. The discrepancy between the two methods arises probably from their different sensitivities to signal quality and antenna characteristics. The Method 1 captures the full structure of the channel in both delay and Doppler domains and is thus more robust to variations in signal amplitude and angular coverage. In contrast, the STFT-based method relies on the time evolution of individual delay taps, which makes it more sensitive to the dynamic range of the receiver and the antenna beam pattern. Weak or undetected taps due to low SNR can lead to an underestimation of the Doppler spread.

It should also be noted that the calculation result is influenced by both the window width and the step size. A step size of about 25 % of the window length offers a good compromise between temporal resolution and estimation variance for the considered V2V scenarios. It mainly affects the smoothness of the results: smaller values mean larger overlaps and more frequent RMS Doppler spread sampling. While mean values stay almost unchanged, the estimates are more stable, and the time evolution smoother. With shorter windows, RMS Doppler spread tends to be overestimated due to limited frequency resolution, whereas longer windows converge to the global estimate of Method 1. Note that changing the window length from 64 bins to 1024 bins causes the RMS Doppler spread mean value to change by only about 13%.

Due to the high speed of CIR measurement and the resulting high correlation of adjacent snapshots, a period of 50 CIR was used to evaluate stationarity regions, which set the measurement interval resolution to 6.25 ms. The Table II clearly shows that the dispersion of values for stationarity regions is relatively large, which is to be expected given the nature of

the measured PDPs. The method used is quite sensitive to the choice of parameters, but for the purpose of comparing the two bands it can serve well.

VI. CONCLUSIONS

A comparison of the 60 GHz and 80 GHz bands leads to the conclusion that the two bands do not differ significantly. This is evident from all graphs. Although short-term changes are often different, their trends are similar. It is clear that both RMS delay and Doppler spreads are smallest when the two cars pass each other. The delay spread at this moment is mainly defined by a strong LOS component, and the Doppler shifts are minimal because the relative velocity is zero at the moment of encounter. It is generally known that a higher RMS Doppler spread leads to shorter time intervals over which the channel remains approximately stationary. This is confirmed by the results shown in the table (RMS Doppler spread vs. stationarity regions). Rapidly changing RMS delay spread leads to short stationarity regions. This is difficult to assess, as the rates of change in Fig. 5 appear to be identical. Certain differences in the results can also be attributed to the unequal radiation characteristics of the antennas in the measurement setup. The different RMS Doppler spread values obtained by Method 1 and Method 2 have been explained and are apparently caused by a shorter data segment for calculation and thus greater sensitivity to noise and other system parameters. The results of the Measurement 1 and 2 shown in Table II show some minor differences resulting from larger number of reflective objects in the second measurement leading to a higher RMS delay spread. It's also likely that the relative speed of the vehicles was in reality slightly higher.

ACKNOWLEDGEMENT

The research described in this paper was financed by the Czech Science Foundation, Project No. 23-04304L, "Multiband prediction of millimeter-wave propagation effects for dynamic and fixed scenarios in rugged time varying environments" and by the National Science Centre, Poland, Project No. 2021/43/I/ST7/03294, through the OPUS-22 (LAP) Call in the Weave Program.

REFERENCES

- [1] A. F. Molisch, C. F. Mecklenbräuker, T. Zemen, A. Prokes, M. Hofer, F. Pasic, and H. Hammoud, "Millimeter-wave V2X channel measurements in urban environments," *IEEE Open Journal of Vehicular Technology*, vol. 6, pp. 520–541, 2025.
- [2] H. Wang, X. Yin, X. Cai, H. Wang, Z. Yu, and J. Lee, "Fading characterization of 73 GHz millimeter-wave V2V channel based on real measurements," in *Communication Technologies for Vehicles*. Cham: Springer International Publishing, 2018, pp. 159–168.
- [3] H. Hammoud, Y. Zhang, Z. Cheng, S. Sangodoyin, M. Hofer, F. Pasic, T. Pohl, R. Závorka, A. Prokeš, T. Zemen, C. F. Mecklenbräuker, and A. F. Molisch, "Double-directional V2V channel measurement using reroma at 60 GHz," *arxiv:2412.01165*, 2024.
- [4] X. Liu, S. Liu, W. Zhou, L. Yang, and G. Yue, "Measurements and modeling of millimeter-wave vehicle-to-vehicle propagation with vehicle obstructions," *IEEE Transactions on Wireless Communications*, vol. 24, no. 5, pp. 4024–4039, 2025.
- [5] A. Ghosh, A. Chandra, T. Mikulasek, A. Prokes, J. Wojtun, J. M. Kelner,

- and C. Ziolkowski, "Vehicle-to-vehicle path loss modeling at millimeter-wave band for crossing cars," *IEEE Antennas and Wireless Propagation Letters*, vol. 22, no. 9, pp. 2125–2129, 2023.
- [6] A. Chopra, A. Thornburg, O. Kanhere, S. S. Ghassemzadeh, M. Majmundar, and T. S. Rappaport, "A real-time millimeter wave V2V channel sounder," in *2022 IEEE Wireless Communications and Networking Conference (WCNC)*, 2022, pp. 2607–2612.
- [7] J. Hoellinger, G. Makhoul, R. D'Errico, and T. Marsault, "V2V dynamic channel characterization in 5G mmWave band," in *2022 International Symposium on Antennas and Propagation (ISAP)*, 2022, pp. 525–526.
- [8] S. Takahashi, A. Kato, K. Sato, and M. Fujise, "Distance dependence of path loss for millimeter wave inter-vehicle communications," in *2003 IEEE 58th Vehicular Technology Conference. VTC 2003-Fall (IEEE Cat. No.03CH37484)*, vol. 1, 2003, pp. 26–30 Vol.1.
- [9] D. Dupleich, R. Müller, S. Skoblikov, C. Schneider, J. Luo, M. Boban, G. Del Galdo, and R. Thomä, "Multi-band characterization of path-loss, delay, and angular spread in V2V links," in *2018 IEEE 29th Annual International Symposium on Personal, Indoor and Mobile Radio Communications (PIMRC)*, 2018, pp. 85–90.
- [10] D. Dupleich, R. Muller, C. Schneider, S. Skoblikov, J. Luo, M. Boban, G. Del Galdo, and R. Thoma, "Multi-band vehicle to vehicle channel measurements from 6 GHz to 60 GHz at "T" intersection," in *2019 IEEE 2nd Connected and Automated Vehicles Symposium (CAVS)*, 2019, pp. 1–5.
- [11] H. Groll *et al.*, "Sparsity in the delay-Doppler domain for measured 60 GHz vehicle-to-infrastructure communication channels," in *2019 IEEE International Conference on Communications Workshops (ICC Workshops)*. Shanghai, China: IEEE, May 2019.
- [12] A. Yamamoto, K. Ogawa, T. Horimatsu, A. Kato, and M. Fujise, "Path-loss prediction models for intervehicle communication at 60 GHz," *IEEE Transactions on Vehicular Technology*, vol. 57, no. 1, pp. 65–78, 2008.
- [13] M. Boban, D. Dupleich, N. Iqbal, J. Luo, C. Schneider, R. Müller, Z. Yu, D. Steer, T. Jämsä, J. Li *et al.*, "Multi-band vehicle-to-vehicle channel characterization in the presence of vehicle blockage," *IEEE Access*, vol. 7, pp. 9724–9735, 2019.
- [14] J. Vychodil, M. Pospisil, A. Prokes, and J. Blumenstein, "Millimetre wave band time domain channel sounder," *IET Communications*, vol. 13, no. 3, pp. 331–338, 2019.
- [15] R. Zavoroka, T. Mikulasek, J. Vychodil, J. Blumenstein, A. Chandra, H. Hammoud, J. M. Kelner, C. Ziolkowski, T. Zemen, C. Mecklenbräuker, and A. Prokes, "Characterizing the 80 GHz channel in static scenarios: Diffuse reflection, scattering, and transmission through trees under varying weather conditions," *IEEE Access*, vol. 12, pp. 144 738–144 749, 2024.
- [16] A. Goldsmith, *Wireless Communications*. New York, USA: Cambridge University Press, 2005.
- [17] L. Bernadó, T. Zemen, F. Tufvesson, A. F. Molisch, and C. F. Mecklenbräuker, "The (in-) validity of the wssus assumption in vehicular radio channels," in *IEEE 23rd International Symposium on Personal, Indoor and Mobile Radio Communications (PIMRC)*. IEEE, 2012, pp. 1757–1762.
- [18] U. Dmitry and M. Patzold, "Stationarity test for wireless communication channels," in *GLOBECOM 2009 - 2009 IEEE Global Telecommunications Conference*, 2009, pp. 1–6.